AGU PUBLICATIONS

Geophysical Research Letters

RESEARCH LETTER
10.1002/2016GL068560

Key Points:
- A 0.3–3% metallic melt can produce the features of the large low shear velocity provinces
- Trapping of metallic melt is likely during the crystallization of a dense basal magma ocean
- Large low shear velocity provinces can become a primordial geochemical mantle reservoir

Supporting Information:
- Supporting Information S1

Correspondence to:
Z. Zhang,
zhan1721@umn.edu

Citation:
Zhang, Z., S. M. Dorfman, J. Labidi, S. Zhang, M. Li, M. Manga, L. Stixrude, W. F. McDonough, and Q. Williams (2016), Primordial metallic melt in the deep mantle, *Geophys. Res. Lett.*, *43*, 3693–3699, doi:10.1002/2016GL068560.

Received 7 MAR 2016
Accepted 29 MAR 2016
Accepted article online 5 APR 2016
Published online 25 APR 2016
Corrected 5 MAY 2016

This article was corrected on 5 MAY 2016. See the end of the full text for details.

Primordial metallic melt in the deep mantle

Zhou Zhang[1], Susannah M. Dorfman[2,3], Jabrane Labidi[4], Shuai Zhang[5], Mingming Li[6,7], Michael Manga[5], Lars Stixrude[8], William F. McDonough[9], and Quentin Williams[10]

[1]Department of Earth Sciences, University of Minnesota, Minneapolis, Minnesota, USA, [2]Earth and Planetary Science Laboratory, Ecole Polytechnique Fédérale de Lausanne, Lausanne, Switzerland, [3]Now at Department of Earth and Environmental Sciences, Michigan State University, East Lansing, Michigan, USA, [4]Geophysical Laboratory, Carnegie Institute of Washington, Washington, District Columbia, USA, [5]Department of Earth and Planetary Science, University of California, Berkeley, California, USA, [6]School of Earth and Space Exploration, Arizona State University, Tempe, Arizona, USA, [7]Now at Department of Physics, University of Colorado Boulder, Boulder, Colorado, USA, [8]Department of Earth Sciences, University College London, London, UK, [9]Department of Geology, University of Maryland, College Park, Maryland, USA, [10]Department of Earth and Planetary Sciences, University of California, Santa Cruz, California, USA

Abstract Seismic tomography models reveal two large low shear velocity provinces (LLSVPs) that identify large-scale variations in temperature and composition in the deep mantle. Other characteristics include elevated density, elevated bulk sound speed, and sharp boundaries. We show that properties of LLSVPs can be explained by the presence of small quantities (0.3–3%) of suspended, dense Fe-Ni-S liquid. Trapping of metallic liquid is demonstrated to be likely during the crystallization of a dense basal magma ocean, and retention of such melts is consistent with currently available experimental constraints. Calculated seismic velocities and densities of lower mantle material containing low-abundance metallic liquids match the observed LLSVP properties. Small quantities of metallic liquids trapped at depth provide a natural explanation for primitive noble gas signatures in plume-related magmas. Our model hence provides a mechanism for generating large-scale chemical heterogeneities in Earth's early history and makes clear predictions for future tests of our hypothesis.

1. Introduction

The origins of the two large low shear velocity provinces (LLSVPs) in the deep mantle beneath Africa and the central Pacific have been enigmatic and controversial since their discovery in seismic tomographic models [*Su et al.*, 1994; *Li and Romanowicz*, 1996]. These features are believed to play a key role in the convective circulation of the deep mantle [e.g., *Davaille*, 1999; *McNamara and Zhong*, 2005; *Deschamps et al.*, 2012]. The colocation of LLSVPs with reconstructed past hotspot locations over the last several hundred million years may account for the primordial geochemical signatures observed in hotspot lavas [*Burke et al.*, 2008; *Torsvik et al.*, 2010; *Jackson and Carlson*, 2011]. Indeed, geodynamic simulations show that large mantle structures can remain stable at the base of the mantle throughout Earth's history if they are denser than the surrounding mantle [*Jellinek and Manga*, 2002; *McNamara and Zhong*, 2005].

Observed characteristics of the LLSVPs, which extend from the core-mantle boundary to heights of 400–1000 km and with breadths on the scale of approximately thousands of kilometers, include depressed shear wave velocity (~3–4% relative to average mantle) [*Garnero*, 2000], elevated density (~1% relative to average mantle) [*Ishii and Tromp*, 1999], possibly elevated bulk sound speed, and sharp boundaries [*Ni et al.*, 2002]. Three scenarios might produce these seismic signatures: a temperature anomaly ~400–800 K hotter than surrounding mantle [*Davies et al.*, 2012]; a variation in major element composition, with modest enrichment in iron and silicon relative to an assumed pyrolitic composition [*Deschamps et al.*, 2012]; or a combination of thermal and chemical effects. Support for higher temperatures in LLSVPs relative to the surrounding mantle includes geodetic evidence for dynamic upwelling [*McNutt*, 1998] and geochemical evidence for plume volcanism above these regions [*Burke et al.*, 2008; *Torsvik et al.*, 2010]. Long-term stability of compositional heterogeneities at the base of the mantle implies that their chemical density, likely due to elevated iron content, exceeds their thermal buoyancy. The sharp boundaries of the LLSVPs and the anticorrelation between shear and bulk sound seismic velocities point to compositional differences [*Su et al.*, 1994], but a composition that matches geophysical observations and a corresponding process that forms large-scale heterogeneities of this composition have not been uniquely identified.

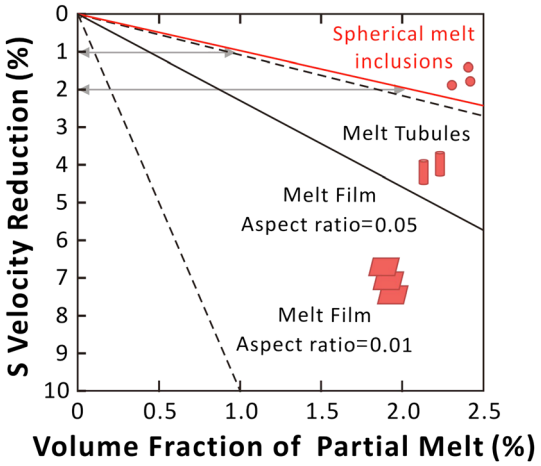

Figure 1. Effect of melt percentage and geometry on shear wave velocity reduction of bulk phase assemblage, based on parameters in the calculation from *Williams and Garnero*, [1996] (see supporting information Text S1 for details).

A few mechanisms have been proposed for generating large-scale chemical heterogeneities early in Earth's history, through the enrichment of Fe, Si, and/or basaltic material [*Christensen and Hofmann*, 1994; *Labrosse et al.*, 2007; *Lee et al.*, 2010; *Deschamps et al.*, 2012]. These models view Fe as sequestered within solid silicates in an oxidized form. Here we propose a new model that is focused on ancient portions of the mantle retaining small quantities of molten, Fe-Ni-S metallic blebs, in a manner analogous to that proposed in the mantle with low oxygen fugacity [*Frost et al.*, 2004; *Rohrbach et al.*, 2007]. Hence, our model differs fundamentally from prior models in its proposed redox state of iron.

2. Our Model

The slow shear wave speed that defines the LLSVPs and inferred elevated temperature are consistent with the presence of a small amount of melt [*Williams and Garnero*, 1996] (Figure 1; see supporting information Text S1 for details). A molten phase in a potentially primordial, undegassed region would store ancient noble gases [*Coltice et al.*, 2011]. The melting points of the major silicate and oxide phases of the lower mantle are, however, too high to permit widespread melting over the large scale of the anomalies (Figure 2 and see supporting information Text S2 for details). In contrast, a separate minor metallic Fe-Ni-S phase would be molten at LLSVP pressures and temperatures (Figure 2 and see supporting information Text S2 for details) and would increase the density of the bulk assemblage (the density of pure Fe alloy is about twice that of ambient silicate mantle). A suspension of small quantities (<3%) of Fe-Ni-S liquid within LLSVPs could thus explain their depressed shear velocities and their location at the base of the mantle. Here we present a process for generating partially molten, Fe-Ni-S liquid-bearing LLSVPs from the differentiation and cooling of the early Earth, and discuss its consistency with geochemical and geophysical constraints.

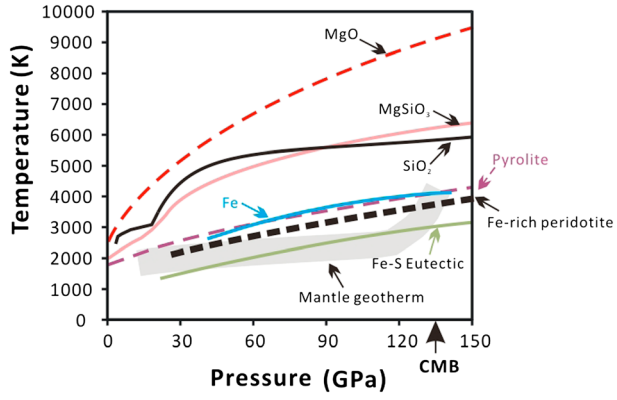

Figure 2. Pressure dependence of melting points of lower mantle components. MgO: *Alfe* [2005]; $MgSiO_3$: *Stixrude and Karki* [2005]; SiO_2: *Usui and Tsuchiya* [2010]; Pyrolite: *Fiquet et al.* [2010]; Fe: *Anzellini et al.* [2013]; Fe-S eutectic: *Kamada et al.* [2012]; and mantle geotherm: *Stixrude et al.* [2009]. Fe-rich peridotite: 400 K lower than pyrolite according to low-pressure (0–10 GPa) studies on the solidus of peridotite with Mg# 90 and Mg# 70 and the fayalite-forsterite binary [*Hirschmann*, 2000; *Wasylenki et al.*, 2003]. CMB stands for core-mantle boundary.

We propose that the crystallization of a basal magma ocean [*Labrosse et al.*, 2007] incorporated inclusions of Fe-Ni-S liquid in a dense cumulate layer, which became the modern LLSVPs. Formation of metal through charge disproportionation of divalent iron represents a separate, complementary possibility for producing a metallic phase [*Frost et al.*, 2004]. The metallic phase contributes to a compositional density anomaly of a few percent. Mantle convection simulations show that a dense basal layer with appropriate viscosity contrasts relative to ambient mantle will be advected into mounds with a pile-like morphology akin to that observed today [*McNamara and Zhong*, 2005; *Davies et al.*, 2012].

3. Consistency With Geophysical Observations

Figure 1 shows the shear velocity depression resulting from small amounts of melt,

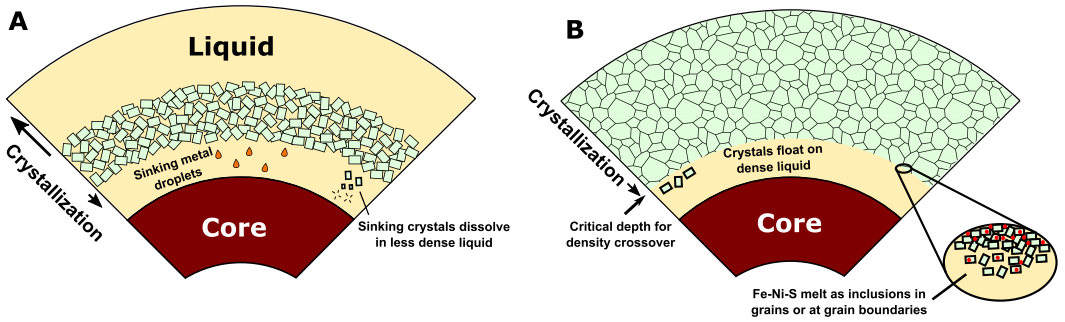

Figure 3. Magma ocean solidification. (a) Initiation of mantle crystallization and segregation of rapidly crystallizing upper magma ocean and slowly crystallizing basal magma ocean. (b) At the density crossover of crystallizing basal magma ocean, floating crystals trap Fe-Ni-S liquid.

based on the elasticity of two-phase aggregates (see supporting information Text S1 for details). The seismic velocity decrement associated with LLSVPs of ~2 (±1)% [*Li and Romanowicz*, 1996; *Ishii and Tromp*, 1999] can be generated by 0.3–3% of trapped iron-rich melt, with values at the low end of this range expected if metallic melt tends to wet grain boundaries [*Shi et al*., 2013]. The presence of 1% pure Fe metal yields a chemical density contrast of ~1%. The estimated density anomaly decreases with increasing light-element content in the Fe-Ni-S liquid and temperature difference relative to the surrounding mantle. For a given amount of iron alloy, and assuming a LLSVP 500 K hotter than its surroundings [*Deschamps et al*., 2012], the density is further reduced by ~0.5% due to thermal expansion and the shear velocity is further reduced by $\delta \ln V_S \sim -1.5\%$ (see supporting information Text S3 for details). The total changes of shear velocity and density of LLSVPs caused by combined compositional and thermal effects are consistent with current models of seismic observations [*Li and Romanowicz*, 1996; *Ishii and Tromp*, 1999]. Other geophysical probes, such as electrical conductivity inversions and neutrino tomography, do not currently constrain the viability of our model due to a lack of spatial resolution in the current observational data set.

4. Dynamic Process

Following the moon-forming impact, the mantle was totally molten [*Nakajima and Stevenson*, 2015]. The segregation of a primordial, dense layer at the base of the mantle may arise from crystallization of a magma ocean. Crystallization has been suggested to begin at midmantle pressures, where the adiabatic temperature profile of the cooling magma ocean intersects the liquidus of the bulk silicate Earth [*Stixrude et al*., 2009], dividing the magma ocean into upper and deeper oceans (Figure 3a). The upper magma ocean will freeze within 10^7 years owing to rapid radiative and convective heat loss to the atmosphere [*Hamano et al*., 2013]. The deeper magma ocean cools much more slowly, as heat loss is limited by solid-state convection in the overlying mantle, with a solidification time of 10^9 years [*Labrosse et al*., 2007] (supporting information Text S4 for details).

During the early stages of deep magma ocean solidification, the precipitation of metal droplets could be driven by a decrease of sulfur solubility in silicate liquid due to cooling ("Hadean matte") [*O'Neill*, 1991] and /or Fe disporportionation through the reaction [$3Fe^{2+}$ (magma) $\leftrightarrow 2Fe^{3+}$ (bridgmanite) + Fe^0 (metallic melt)] at oxygen fugacities near iron-wüstite-2 [*Frost et al*., 2004]. Once Fe precipitates from the silicate liquid, Ni and light elements (such as S, C, and O) will concentrate in this phase. Assuming sulfur saturation in the silicate liquid (~400 μg/g) implies that the (Fe + Ni)/S atomic ratio ranges from 3 to 100. The possible presence of other lighter alloying components (such as oxygen or carbon) within these is, however, neither mandated nor precluded (see supporting information Text S5 for details).

Both the crystals and Fe-Ni-S liquids that exsolve during crystallization are denser than the residual melt. Sinking crystals move to conditions above their melting points and should redissolve into the magma ocean. For metal droplets to settle to the core, they must be large enough to settle faster than the speeds of both the solidification front and the velocity fluctuations in the convecting magma ocean. Experimental observations suggest that exsolved metallic melt droplets initially have radii $r_0 \sim 10^{-6}$ m, giving an expected

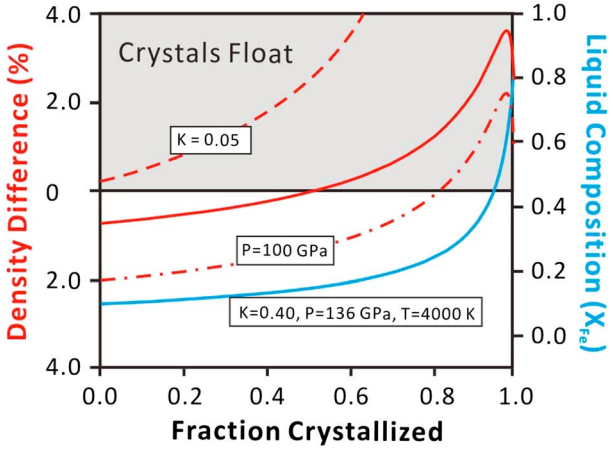

Figure 4. Melt composition and density evolution. Variation of the liquid-solid density contrast (bold red) and liquid composition (blue) at 136 GPa and 4000 K, assuming a value of the Mg-Fe solid-liquid partition coefficient $K = 0.4$ [*Andrault et al.*, 2012]. Also shown are the density contrasts computed for an alternate value of pressure (100 GPa) and partition coefficient ($K = 0.05$) [*Nomura et al.*, 2011]. The density of liquid and crystalline phases is computed following the method of *Muñoz Ramo and Stixrude* [2014] (see supporting information Text S9 for details). Metallic melt precipitation drives the density contrast curves left, reaching the crystal-liquid density crossover at shallower depth.

settling rate of $u_s \sim 10^{-8}$ m/s. Although u_s exceeds the speed at which the solidification front moves downward, 10^{-10} m/s, it is small relative to convective velocities in the magma ocean, 10^{-2} m/s, and the magnitude of velocity fluctuations at the Kolmogorov scale, 10^{-4} m/s (see supporting information Text S6 for details). Droplets will coalesce as they sink under the influence of gravity and as they are brought into contact by flow in the convecting magma ocean. Droplets will grow to reach radii large enough that their settling speed exceeds the convective velocity over short time scales, 10^3 to 10^6 s (see supporting information Text S6 for details). Although both inertial forces and turbulent stress fluctuations will limit the maximum size of droplets to about 10^{-3} to 10^{-2} m, droplets of this size are still larger than the minimum required to sink to the core. Thus, at this stage, the crystallizing lower mantle is nearly free of metallic Fe-Ni-S liquids (see supporting information Text S7 for details).

A density crossover in the magma ocean near the end of its solidification allows metallic melt droplets to be trapped within floating, crystallizing silicates (see supporting information Text S8 and Text S9 for details) (Figure 3b). At a critical depth that depends on composition and melt-silicate partitioning, the residual silicate melt becomes denser than the crystallizing phases (see supporting information Text S9 for details). With the crystallization of residual silicate melt, the bridgmanite and ferropericlase crystals are enriched in Fe compared with the bulk silicate Earth, increasing their bulk moduli and providing a possible explanation for the elevated bulk modulus of LLSVPs (Figure 4). The buoyant crystals may then trap metal droplets formed at the solidification front at grain boundaries (see supporting information Text S8 for details). Laboratory experiments suggest that metal may wet bridgmanite at high pressure, allowing metal to drain [*Shi et al.*, 2013]. Wetting behavior strongly depends on the sample environment [*Walte et al.*, 2011; *Ghanbarzadeh et al.*, 2015], and the role of nonhydrostatic experimental conditions in generating connectivity in bridgmanite-metal aggregates remains unclear. Within the pioneering experiments of *Shi et al.* [2013], a few percent of the metal remains as isolated droplets, and even wetting fluids are commonly trapped as fluid inclusions during crystal growth [*Shaw and Duncombe*, 1991]. Other factors such as low permeability and surface tension will generate a strong force resisting complete draining of small amount of liquid at solid silicate grain boundaries (see supporting information Text S8 for details) [*Belien et al.*, 2010; *Holtzman*, 2016]. Experiments also suggest that deformation with silicate liquid present does not promote the drainage of the metal or sulfide component [*Cerantola et al.*, 2015]. Thus, even if the bulk of the metallic component is lost, a small volume fraction of a few percent metallic melt may still remain trapped as isolated droplets, likely with high aspect ratios as in *Shi et al.* [2013]. Alternatively, if the magma ocean solidifies from the core-mantle boundary upward, exsolved metal will be trapped with the minerals that crystallize at or near the crystal-liquid interface: any deep crystal-liquid density crossover [*Muñoz Ramo and Stixrude*, 2014] will facilitate this trapping. Sharp boundaries separating metal-rich and metal-poor regions might then be associated with depth-varying changes in redox state.

5. Consistency With Geochemical Observations

The metallic melt droplets are Fe-Ni-S liquids, which might contain up to 10^1 to 10^4 higher concentrations of platinum group elements (PGEs) and Ni than ambient mantle (see supporting information Text S10 for

details). Because LLSVPs comprise 10^{-2} to 10^{-1} of the whole mantle, and the metallic melt is ~10^{-2} of the LLSVPs in our model, these abundances have small effects on the composition of hot spot magmas that might sample LLSVPs: accordingly, they also do not alter the global volatility trend of these elements within the bulk Earth (see supporting information Text S10 for details).

Our calculations thus suggest that the Fe-Ni-S liquid is not expected to create resolvable PGEs and Ni anomalies nor W isotope anomalies (see supporting information Text S10 for details). However, Fe-Ni-S liquid or silicate/oxide crystals in LLSVPs might contain primordial noble gas compositions with significant differences from ambient mantle. Despite being the most studied noble gas, little is known about helium partitioning between silicate solids/silicate melt or silicate solids/metallic melt under relevant lower mantle pressures and temperatures. Both Fe-Ni-S liquid and its adjacent silicate crystals are potential candidates noble gas carriers, depending on their noble gas solubility (Figure S2). On the one hand, if helium is preferentially partitioned into Fe-Ni-S liquid, the Fe-Ni-S liquid could potentially store significant primordial noble gases compared with silicate crystals [*Heber et al*., 2007*; Bouhifd et al*., 2013; *Huang et al.*, 2014]. On the other hand, if noble gases were to have higher silicate solid/liquid partition coefficients at high pressure (e.g., Xe: *Sanloup et al*. [2011]), they could be stored in silicate phases rather than Fe-Ni-S liquids. In this scenario, the droplet occurrence would only have acted as a physical mechanism to isolate the LLSVP from whole mantle convection (through a density increase) but not as the host of the noble gases (especially Xe). In both cases, the occurrence of the metallic droplets creates the geological context preservation of the primordial noble gas signatures in LLSVPs.

Mechanical entrainment by upwellings, from either the sides or top of the LLSVPs, provides the mechanism that delivers material containing primordial noble gas signatures from depth to hotspot-related surface volcanism. Furthermore, it is noteworthy that the reconstructed eruption of lavas that have high $^{3}He/^{4}He$ ratios (as well as primordial Ne, Ar, and Xe isotope compositions) [*Mukhopadyay*, 2012] lie close to, or within, the inferred boundaries of the African (for which low velocities extend substantially north beneath the Atlantic to near Icelandic latitudes) or Pacific LLVSPs [*Lekic et al*., 2012; *Rickers et al*., 2013].

6. Discussion

Recent compositional models of LLSVPs have proposed that a combination of iron and $(Mg,Fe)SiO_3$-bridgmanite enrichment (~3% and 18%, respectively) could explain their observed seismic velocity and density characteristics [*Deschamps et al*., 2012]. However, how such compositions might be generated in the deep Earth remains enigmatic (see supporting information Text S11 for details). There is also the possibility that small amounts of silicate liquids might be present within LLSVPs [e.g., *Lay et al*., 2004]. Such silicate liquids, however, would be expected to equilibrate with their coexisting solids, and current estimates of iron partitioning in natural assemblages coupled with inferred volumes of fusion indicate that such liquids would be generally similar in density to their coexisting solids [e.g., *Andrault et al*., 2012]. Therefore, producing the apparently elevated density of LLSVP's via silicate melting would involve amounts of liquid that are incompatible with the observed shear wave velocities.

The metallic melt model, using a single compositional component that can arise through the simple mechanism of trapping and inefficient extraction of iron from portions of the mantle, quantitatively explains known LLSVP properties: the decrement of shear velocity, a small density increase (in accord with current seismic constraints), and sharp edges of these features. From a geochemical perspective, the presence of Fe-Ni-S liquid or adjacent silicate and oxide crystals in LLSVPs also provides a plausible location to store incompatible noble gases.

Our hypothesis can be tested by a combination of future geophysical observations and laboratory studies (see supporting information Text S12 for details). Specifically, the model makes a clear prediction for the relationship between density and seismic anomalies and implies locally increased electrical conductivity. Laboratory experiments can also provide tests of some of the features built into the evolutionary model for creating LLSVPs. Constraints that are needed are (1) noble gas partitioning experiments at ~100 GPa to quantify partitioning between silicate crystals, metallic melt, and silicate melt; (2) experiments with silicate liquids with a range of compositions at lower mantle pressures, temperatures, and oxygen fugacity to quantify Fe-Ni-S liquid amount and composition; (3) an accurate oxygen fugacity depth profile in the magma ocean to constrain the amount of metal precipitation in the whole mantle; (4) quantifying wetting behavior

of metallic melt in polyphase assemblages that include ferropericlase and $CaSiO_3$-perovskite at low stress conditions; and (5) identifying physical mechanism separate Fe-Ni-S liquid from percolation (e.g., silicate crystal annealing) at lower mantle conditions.

7. Concluding Remarks

The genesis of Fe-Ni-S liquid features is a natural consequence of the solidification of an early, deep magma ocean: dynamic constraints show that trapping and retaining small amounts of Fe-Ni-S liquids are likely to occur during and following the solidification of a magma ocean. Retention of minor amounts of Fe-Ni-S liquids in silicates is compatible with current experimental constraints, particularly given uncertainties about the role of nonhydrostatic stresses. The model further suggests that small quantities of Fe-Ni-S liquids trapped at depth have limited impact on the siderophile element budget of the planet and predicts that LLSVP material, if entrained within upwellings, would manifest itself as a high $^3He/^4He$ component in magmas. Finally, Fe-Ni-S liquid enrichment in LLSVPs implies that these features are primordial, long-lived, and chemically reduced and that they are our planet's only known manifestation of incomplete segregation of Fe-Ni-S liquids into Earth's core.

Acknowledgments

We thank Cin-ty Lee and another anonymous reviewer for their constructive comments. This manuscript originated from a project group discussion at the 2014 CIDER summer program at the Kavli Institute of Theoretical Physics at the University of California at Santa Barbara. We pay tribute to Adam Dziewonski, a member of the CIDER founding team. We acknowledge the leadership of Barbara Romanowicz and all participants in the program for feedback. We thank Dan Frost for discussion. CIDER was supported by the NSF Frontiers of Earth Systems Dynamics grant EAR-1135452. L.S. was supported by the European Research Council under advanced grant 291432 "Molten Earth" (FP7/2007-2013). S.D. thanks the Marie Heim-Vögtlin program of the Swiss National Science Foundation for support through project PMPDP2_151256. J.L. was supported by a Carnegie (Geophysical Laboratory) postdoctoral fellowship. M.M. was supported by the NSF under grant EAR-1135382. Q.W. was supported by the NSF under grant EAR-1215745. Z.Z. was supported by the NSF under grant EAR-1426772.

References

Alfè, D. (2005), Melting curve of MgO from first-principles simulations, *Phys. Rev. Lett.*, *94*, 23,5701.

Andrault, D., S. Petitgirard, G. Lo Nigro, J.-L. Devidal, G. Veronesi, G. Garbarino, and M. Mezouar (2012), Solid-liquid iron partitioning in Earth's deep mantle, *Nature*, *487*, 354–357.

Anzellini, S., A. Dewaele, M. Mezouar, P. Loubeyre, and G. Morard (2013), Melting of iron at Earth's inner core boundary based on fast X-ray diffraction, *Science*, *340*, 464–466.

Belien, I. B., K. V. Cashman, and A. W. Rempel (2010), Gas accumulation in particle-rich suspensions and implications for bubble populations in crystal-rich magma, *Earth Planet. Sci. Lett.*, *297*, 133–140.

Bouhifd, M. A., A. P. Jephcoat, V. S. Heber, and S. P. Kelley (2013), Helium in Earth's early core, *Nat. Geosci.*, *6*, 982–986.

Burke, K., B. Steinberger, T. H. Torsvik, and M. A. Smethurst (2008), Plume generation zones at the margins of large low shear velocity provinces on the core–mantle boundary, *Earth Planet. Sci. Lett.*, *265*, 49–60.

Cerantola, V., N. P. Walte, and D. C. Rubie (2015), Deformation of a crystalline olivine aggregate containing two immiscible liquids: Implications for early core–mantle differentiation, *Earth Planet. Sci. Lett.*, *417*, 67–77.

Christensen, U. R., and A. W. Hofmann (1994), Segregation of subducted oceanic crust in the convecting mantle, *J. Geophys. Res.*, *99*, 19,867–19,884, doi:10.1029/93JB03403.

Coltice, N., M. Moreira, J. Hernlund, and S. Labrosse (2011), Crystallization of a basal magma ocean recorded by helium and neon, *Earth Planet. Sci. Lett.*, *308*, 193–199.

Davaille, A. (1999), Simultaneous generation of hotspots and superswells by convection in a heterogeneous planetary mantle, *Nature*, *402*, 756–760.

Davies, D. R., S. Goes, J. H. Davies, B. S. A. Schuberth, H.-P. Bunge, and J. Ritsema (2012), Reconciling dynamic and seismic models of Earth's lower mantle: The dominant role of thermal heterogeneity, *Earth Planet. Sci. Lett.*, *353–354*, 253–269.

Deschamps, F., L. Cobden, and P. J. Tackley (2012), The primitive nature of large low shear-wave velocity provinces, *Earth Planet. Sci. Lett.*, *349–350*, 198–208.

Fiquet, G., A. L. Auzende, J. Siebert, A. Corgne, H. Bureau, H. Ozawa, and G. Garbarino (2010), Melting of peridotite to 140 gigapascals, *Science*, *329*, 1516–1518.

Frost, D. J., C. Liebske, F. Langenhorst, C. A. McCammon, R. G. Trønnes, and D. C. Rubie (2004), Experimental evidence for the existence of iron-rich metal in the Earth's lower mantle, *Nature*, *428*, 409–412.

Garnero, E. J. (2000), Heterogeneity of the lowermost mantle, *Annu. Rev. Earth Planet. Sci.*, *28*, 509–537.

Ghanbarzadeh, S., M. A. Hesse, M. Prodanovic, and J. E. Gardner (2015), Deformation-assisted fluid percolation in rock salt, *Science*, *350*, 1069–1072.

Hamano, K., Y. Abe, and H. Genda (2013), Emergence of two types of terrestrial planet on solidification of magma ocean, *Nature*, *497*, 607–610.

Heber, V. S., R. A. Brooker, S. P. Kelley, and B. J. Wood (2007), Crystal–melt partitioning of noble gases (helium, neon, argon, krypton, and xenon) for olivine and clinopyroxene, *Geochim. Cosmochim. Acta*, *71*, 1041–1061.

Hirschmann, M. (2000), Mantle solidus: Experimental constraints and the effects of peridotite composition, *Geochem. Geophys. Geosyst.*, *1*(10), 1042, doi:10.1029/2000GC000070.

Holtzman, B. (2016), Questions on the existence, persistence, and mechanical effects of a very small melt fraction in the asthenosphere, *Geochem. Geophys. Geosyst.*, *16*, 470–484, doi:10.1002/2015GC006102.

Huang, S., C.-T. A. Lee, and Q. Z. Yin (2014), Missing lead and high $^3He/^4He$ in ancient sulfides associated with continental crust formation, *Sci. Rep.*, *4*, 5314.

Ishii, M., and J. Tromp (1999), Normal-mode and free-air gravity constraints on lateral variations in velocity and density of Earth's mantle, *Science*, *285*, 1231–1236.

Jackson, M. G., and R. W. Carlson (2011), An ancient recipe for flood-basalt genesis, *Nature*, *476*, 316–319.

Jellinek, A. M., and M. Manga (2002), The influence of a chemical boundary layer on the fixity, spacing and lifetime of mantle plumes, *Nature*, *418*, 760–763.

Kamada, S., E. Ohtani, H. Terasaki, T. Sakai, M. Miyahara, Y. Ohishi, and N. Hirao (2012), Melting relationships in the Fe–Fe_3S system up to the outer core conditions, *Earth Planet. Sci. Lett.*, *359–360*, 26–33.

Labrosse, S., J. W. Hernlund, and N. Coltice (2007), A crystallizing dense magma ocean at the base of the Earth's mantle, *Nature*, *450*, 866–869.

Lay, T., E. J. Garnero, and Q. Williams (2004), Partial melting in a thermochemical boundary layer at the base of Earth's mantle, *Phys. Earth Planet. Inter.*, *146*, 441–467.

Lee, C.-T. A., P. Luffi, T. Höink, J. Li, R. Dasgupta, and J. Hernlund (2010), Upside-down differentiation and generation of a 'primordial' lower mantle, *Nature*, *463*, 930–933.
Lekic, V., S. Cottaar, A. Dziewonski, and B. Romanowicz (2012), Cluster analysis of global lower mantle tomography: A new class of structure and implications for chemical heterogeneity, *Earth Planet. Sci. Lett.*, *357–358*, 68–77.
Li, X.-D., and B. Romanowicz (1996), Global mantle shear velocity model developed using nonlinear asymptotic coupling theory, *J. Geophys. Res.*, *101*, 22,245–22,272, doi:10.1029/96JB01306.
McNamara, A. K., and S. Zhong (2005), Thermochemical structures beneath Africa and the Pacific Ocean, *Nature*, *437*, 1136–1139.
McNutt, M. K. (1998), Superswells, *Rev. Geophys.*, *36*, 211–244, doi:10.1029/98RG00255.
Mukhopadyay, S. (2012), Early differentiation and volatile accretion recorded in deep-mantle neon and xenon, *Nature*, *486*, 101–104.
Muñoz Ramo, D., and L. Stixrude (2014), Spin crossover in Fe_2SiO_4 liquid at high pressure, *Geophys. Res. Lett.*, *41*, 4512–4518, doi:10.1002/2014GL060473.
Nakajima, M., and D. J. Stevenson (2015), Melting and mixing states of the Earth's mantle after the Moon-forming impact, *Earth Planet. Sci. Lett.*, *427*, 286–295.
Ni, S. D., E. Tan, M. Gurnis, and D. V. Helmberger (2002), Sharp sides to the African superplume, *Science*, *296*, 1850–1852.
Nomura, R., H. Ozawa, S. Tateno, K. Hirose, J. Hernlund, S. Muto, H. Ishii, and N. Hiraoka (2011), Spin crossover and iron-rich silicate melt in the Earth's deep mantle, *Nature*, *473*, 199–202.
O'Neill, H. St. C. (1991), The origin of the Moon and the early history of the Earth – A chemical model. Part 2: The Earth, *Geochim. Cosmochim. Acta*, *55*, 1159–1172.
Rickers, F., A. Fichtner, and J. Trampert (2013), The Iceland–Jan Mayen plume system and its impact on mantle dynamics in the North Atlantic region: Evidence from full-waveform inversion, *Earth Planet. Sci. Lett.*, *367*, 39–51.
Rohrbach, A., C. Ballhaus, U. Golla-Schindler, P. Ulmer, V. S. Kamenetsky, and D. V. Kuzmin (2007), Metal saturation in the upper mantle, *Nature*, *449*, 456–458.
Sanloup, C., B. C. Schmidt, G. Gudfinnsson, A. Dewaele, and M. Mezouar (2011), Xenon and Argon: A contrasting behaviour in olivine at depth, *Geochim. Cosmochim. Acta*, *75*, 6271–6284.
Shaw, T. M., and P. R. Duncombe (1991), Forces between aluminum oxide grains in a silicate melt and their effect on grain boundary wetting, *J. Am. Ceram. Soc.*, *74*, 2495–2505.
Shi, C. Y., L. Zhang, W. Yang, Y. Liu, J. Wang, Y. Meng, J. C. Andrews, and W. L. Mao (2013), Formation of an interconnected network of iron melt at Earth's lower mantle conditions, *Nat. Geosci.*, *6*, 971–975.
Stixrude, L., and B. Karki (2005), Structure and freezing of $MgSiO_3$ liquid in Earth's lower mantle, *Science*, *310*, 297–299.
Stixrude, L., N. de Koker, N. Sun, M. Mookherjee, and B. B. Karki (2009), Thermodynamics of silicate liquids in the deep Earth, *Earth Planet. Sci. Lett.*, *278*, 226–232.
Su, W.-J., R. L. Woodward, and A. M. Dziewonski (1994), Degree 12 model of shear velocity heterogeneity in the mantle, *J. Geophys. Res.*, *99*, 6945–6980, doi:10.1029/93JB03408.
Torsvik, T. H., K. Burke, B. Steinberger, S. J. Webb, and L. D. Ashwal (2010), Diamonds sampled by plumes from the core–mantle boundary, *Nature*, *466*, 352–355.
Usui, Y., and T. Tsuchiya (2010), Ab initio two-phase molecular dynamics on the melting curve of SiO_2, *J. Earth Sci.*, *21*, 801–810.
Walte, N. P., D. C. Rubie, P. D. Bons, and D. J. Frost (2011), Deformation of a crystalline aggregate with a small percentage of high-dihedral-angle liquid: Implications for core–mantle differentiation during planetary formation, *Earth Planet. Sci. Lett.*, *305*, 124–134.
Wasylenki, L. E., M. B. Baker, A. J. R. Kent, and E. M. Stolper (2003), Near-solidus melting of the shallow upper mantle: Partial melting experiments on depleted peridotite, *J. Petrol.*, *44*, 1163–1191.
Williams, Q., and E. Garnero (1996), Seismic evidence for partial melt at the base of Earth's mantle, *Science*, *273*, 1528–1530.

Erratum

In the originally published version of this article, text was inadvertently omitted from section 4 of the main article and from text S5 of the supporting information. These omissions have since been corrected, and this version may be considered the authoritative version of record.

In the second paragraph of section 4, "decrease of solubility" has been corrected to read "decrease of sulfur solubility."

In the first paragraph of text S5 in the supporting information, "Fe solubility" has been corrected to read "sulfur solubility."